IOSR Journal of Electrical and Electronics Engineering (IOSR-JEEE)
e-ISSN: 2278-1676, p-ISSN: 2320-3331, Volume 17, Issue 3 Ser. I (May. – June. 2022), PP 23-42
www.iosrjournals.org

A hybrid Firefly and Particle Swarm Optimized FOF-PID Strategy for Interconnected Multi-area Power System with Renewable Energy Sources

Gomaa Haroun A. H.[1,*], Khaled Eltag[2], Mustafa Eltigani I. M.[3]
[1] *College of Engineering Sciences, Department of Electrical and Electronics Engineering, University of Nyala, South Darfur, Nyala, Sudan*
[2]*Electrical Engineering Department, Omdurman Islamic University, Omdurman, Sudan*
[3] *Department of Electrical Engineering, Delhi Technological University, Delhi, India*
** Corresponding author: Gomaa Haroun (E-mail: gomaaharoun1982@yahoo.com)*

Abstract:
This article presents optimal load frequency control (LFC) designed by a hybrid fractional order fuzzy PID (FOF-PID) controller trained via a hybrid firefly and particle swarm optimization (hFA-PSO) algorithm for multi-interconnected power system be made up of renewable energy sources (RESs). Four-area interconnected power systems comprising from hydro, thermal, photovoltaic (PV) and wind power plants are considered. A hFA-PSO is employed to explore the optimal gains of fractional order fuzzy PID (FOF-PID) controller such that the integral time square error (ITSE) criteria of frequency and tie line power deviations is diminished. Different simulations are carried out and the results are compared with the proposed controller optimized via hFA-PSO, craziness particle swarm optimization (CPSO), PSO and firefly algorithm (FA). It is observed that the suggested controller optimized via hFA-PSO techniques is robust and achieves satisfactorily results even if the plant including nonlinearity as well as varying in operating load condition and plant parameters. The obtained results confirmed the accuracy and reliability of the proposed FOF-PID controller-based hFA-PSO in designing LFC for multi-interconnected power systems compared to others.

Key Word*: Load frequency control (LFC), Interconnected multi-area power systems, fractional order fuzzy PID controller, Firefly algorithm.*

Date of Submission: 28-05-2022 Date of Acceptance: 10-06-2022

I. Introduction

The main aim of the power system (PS) utility is to maintain continuous supply of electrical power within an acceptable quality, to all the consumers in the network. The PS will be in equilibrium, when there is a balance between electrical power demand and the power generated. Load frequency control (LFC) is an external strategy used in an interconnected system to maintain the frequency and tie-line power within their specified limits in case of load perturbation [1]. LFC is continuously observing the system frequency and calculate the net deviations of same from their prescribed values of the area control error (ACE), and accordingly adjust the valve settings of generators so as to maintain ACE to its minimum value [2,3]. It is observed from the literature that there are countless classical and advanced controllers have been approved for LFC problem [1-8]. In [4], the authors designed structure of fuzzy PID controller for an interconnected complex PS, in which the controller gains are tuned using Firefly algorithm (FA). In [5], fuzzy-PI controller is proposed for load frequency control of a hybrid system comprising from PV and thermal generator to improve the dynamic performance. Recently, fractional Order PID (FOPID) is introduced in the control system, which is a generalized type of the classical PID controller [7]. Regarding this controller, the derivative and integrator parts have non-integer orders; therefore the order should be determined by the designer.

This article presents a hybrid fractional order fuzzy PID (FOF-PID) controller for interconnected complex-area power system, where each control area made up of different generation units such as; thermal, hydro, and renewable energy sources (RESs). RESs interconnected power plant may be wind turbine (WT), photovoltaic (PV), and fuel cell (FC), these energies has gained a great attention and have widely prevalence in electrical power plants due to the harmful effects of fossil fuels [8]. The controller gains of the proposed strategy are optimized via a hybrid firefly and particle swarm optimization (hFA-PSO) algorithm.

The following are the main contributions of this article:

1. A new structure of fractional order based hybrid fuzzy PID controller is proposed for LFC of interconnected multi-area power system,
2. A hybrid firefly and particle swarm optimization (hFA-PSO) algorithm is adopted to optimize the controller gains,
3. The effectiveness of the proposed controller is assessed by comparing the results with different optimization techniques; hFA-PSO, CPSO, and PSO.
4. Sensitivity analysis is carried out to prove the robustness of the advocated strategy.

The remainder sections of this article are prepared as follows: The mathematical modeling of the proposed system is addressed in Section 2, followed by wind turbine and PV system modeling. Controller structure is elaborated in Section 3. The overview of hFA-PSO is stated in Section 4 followed by the objective function. Simulation results and comparative analysis are presented in Section 5. Finally, the conclusion of the article was presented in Section 6.

II. System Modelling

2. System under study

Two types of power system configurations have been studied in this article: Configuration 1: Two-area interconnected power systems; area-1 comprises from thermal power plant and area-2 comprises from photovoltaic (PV) power plant. Configuration 2: Four-area interconnected power plants; every area comprises from multi-source; namely: thermal, hydro, wind and photovoltaic (PV) power plants.

2.1. Nonrenewable energy sources

Figs. 1 and 2 show the dynamic structures of nonrenewable energy sources represented in thermal and hydro power plants; respectively. The thermal power plant as offered in Fig. 1, is composed from speed governing, reheat time delay, turbine system, and power plant unit. So, the state space model of the plant can be directly derived from the block diagram. The turbine system can be derived as:

$$\Delta \dot{P}_{gi} = -\frac{1}{T_{ti}}\Delta P_{gi} + \frac{1}{T_{ti}}\Delta P_{ri} \quad (1)$$

where, T_{ti} denotes the reheat turbine time constant (s); ΔP_{gi} is the generator output power error (p.u. MW). The linearization of the speed governing can be derived as:

$$\Delta \dot{X}_{gi} = -\frac{1}{T_{gi}R_i}\Delta f_i - \frac{1}{T_{gi}}\Delta X_{gi} + \frac{1}{T_{gi}}\Delta P_{ci} \quad (2)$$

where, ΔX_{gi} designates as the governor valve position error (p.u), ΔP_{ci} is the control signal, T_{gi} implies the thermal governor time constant, and R_i signifies the speed drop (Hz/p.u. MW). The linearization of the reheat time delay can be derived as:

$$\Delta \dot{P}_{ri} = -\frac{K_{ri}}{T_{gi}R_i}\Delta f_i + \left(\frac{1}{T_{ri}} - \frac{K_{ri}}{T_{gi}}\right)\Delta X_{gi} - \frac{1}{T_{ri}}\Delta P_{ri} \quad (3)$$

The hydro-power system as displayed in Fig. 2, is constructed from speed governing, hydraulic turbine unit, water dynamic system, and power system unit. Thus, the state space model of the plant can be directly derived from the block diagram. The linearization model of water dynamic can be derived as:

$$\Delta \dot{P}_{gi} = 2\left\lfloor\frac{T_{Ri}}{T_{1i}T_{2i}R_i}\right\rfloor\Delta f_i - \frac{2}{T_{wi}}\Delta P_{gi} + 2\left\lfloor\frac{T_{2i}+T_{wi}}{T_{2i}T_{wi}}\right\rfloor\Delta X_{gi} + 2\left\lfloor\frac{T_{Ri}-T_{1i}}{T_{1i}T_{2i}R_i}\right\rfloor\Delta X_{gi} \quad (4)$$

The linearization model of the speed governing can be modeled as:

$$\Delta \dot{X}_{gi} = -\left\lfloor\frac{T_{Ri}}{T_{1i}T_{2i}R_i}\right\rfloor\Delta f_i - \frac{1}{T_{2i}}\Delta X_{gi} - \frac{T_{Ri}-T_{1i}}{T_{1i}T_{2i}R_i}\Delta X_{ghi} \quad (5)$$

The linearization model of the turbine unit can be expressed as:

$$\Delta \dot{X}_{ghi} = -\frac{1}{T_{1i}R_i}\Delta f_i - \frac{1}{T_{1i}}\Delta X_{ghi} \quad (6)$$

The frequency deviation (Δf_i) for each control area $i(i = 1, 2, 3, 4)$ can be expressed as:

$$\Delta \dot{f}_i = -\frac{1}{T_{pi}}\Delta f_i - \frac{K_{pi}}{T_{pi}}\Delta P_{tie,i} + \frac{K_{pi}}{T_{pi}}\Delta P_{gi} - \frac{K_{pi}}{T_{pi}}\Delta P_{Li} \quad (7)$$

where, Δf_i denotes the frequency error (Hz); $\Delta P_{tie,i}$ is the tie-line power deviation (p.u. MW); ΔP_{Li} is the load perturbation (p.u. MW); T_{pi} is the power system time constant (s) and K_{pi} is the power plant gain (Hz/p.u. MW).

The transmission-line power interchange between areas i and j can be describe as

$$\Delta \dot{P}_{tie,ij} = 2\pi T_{ij}\left(\Delta f_i - \Delta f_j\right), \qquad \Delta P_{tie,ij} = -\Delta P_{tie,ji} \tag{8}$$

The total transmission-line power between area-i and the other areas can be formulated as:

$$\Delta \dot{P}_{tie,i} = \sum_{\substack{j=1 \\ j\neq i}}^{4} \Delta P_{tie,ij} = 2\pi \sum_{\substack{j=1 \\ j\neq i}}^{4} T_{ij}\left(\Delta f_i - \Delta f_j\right) \tag{9}$$

The linearized mathematical modeling of each of the 4-areas can be described with following two equations:

$$\begin{cases} \dot{x}_i(t) = A_i x_i(t) + B_i u_i(t) + \mathrm{D}_i w_i(t) + \sum_{\substack{i\neq j \\ j=1}} \left(A_{ij} x_j(t)\right) \\ y_i(t) = C_i x_i(t) \end{cases} \tag{10}$$

The state space model for thermal plant as highlighted in Fig. 1 can be formulated as:

$$x_i(t) = \begin{bmatrix} \Delta f_i(t) \\ \Delta P_{tie,i}(t) \\ \Delta P_{gi}(t) \\ \Delta X_{gi}(t) \\ \Delta P_{ri}(t) \end{bmatrix}, A_i = \begin{bmatrix} -\frac{1}{T_{pi}} & -\frac{K_{pi}}{T_{pi}} & \frac{K_{pi}}{T_{pi}} & 0 & 0 \\ 2\pi\sum_j T_{ij} & 0 & 0 & 0 & 0 \\ 0 & 0 & -\frac{1}{T_{ti}} & 0 & \frac{1}{T_{ti}} \\ -\frac{1}{T_{gi}R_i} & 0 & 0 & -\frac{1}{T_{gi}} & 0 \\ -\frac{K_{ri}}{T_{gi}R_i} & 0 & 0 & \frac{1}{T_{ri}} - \frac{K_{ri}}{T_{gi}} & -\frac{1}{T_{ri}} \end{bmatrix}, B_i = \begin{bmatrix} 0 \\ 0 \\ 0 \\ \frac{1}{T_{gi}} \\ 0 \end{bmatrix}, D_i = \begin{bmatrix} -\frac{K_{pi}}{T_{pi}} \\ 0 \\ 0 \\ 0 \\ 0 \end{bmatrix}$$ and $C_i = [B_i \quad 1 \quad 0 \quad 0 \quad 0]$

The state space model for hydro plant as highlighted in Fig. 2 can be formulated as:

$$x_i(t) = \begin{bmatrix} \Delta f_i(t) \\ \Delta P_{tie,i}(t) \\ \Delta P_{gi}(t) \\ \Delta X_{gi}(t) \\ \Delta X_{ghi}(t) \end{bmatrix}, A = \begin{bmatrix} -\frac{1}{T_{pi}} & -\frac{K_{pi}}{T_{pi}} & \frac{K_{pi}}{T_{pi}} & 0 & 0 \\ 2\pi\sum_j T_{ij} & 0 & 0 & 0 & 0 \\ 2\left[\frac{T_{Ri}}{T_{1i}T_{2i}R_i}\right] & 0 & -\frac{2}{T_{wi}} & 2\left[\frac{T_{2i}+T_{wi}}{T_{2i}T_{wi}}\right] & 2\left[\frac{T_{Ri}-T_{1i}}{T_{1i}T_{2i}R_i}\right] \\ -\left[\frac{T_{Ri}}{T_{1i}T_{2i}R_i}\right] & 0 & 0 & -\frac{1}{T_{2i}} & -\left[\frac{T_{Ri}-T_{1i}}{T_{1i}T_{2i}R_i}\right] \\ -\frac{1}{T_{1i}R_i} & 0 & 0 & 0 & -\frac{1}{T_{1i}} \end{bmatrix}, B_i = \begin{bmatrix} 0 \\ 0 \\ -2R_i\left[\frac{T_{Ri}}{T_{1i}T_{2i}R_i}\right] \\ R_i\left[\frac{T_{Ri}}{T_{1i}T_{2i}R_i}\right] \\ \frac{1}{T_{1i}} \end{bmatrix}, D_i = \begin{bmatrix} -\frac{K_{pi}}{T_{pi}} \\ 0 \\ 0 \\ 0 \\ 0 \end{bmatrix}$$ and

$C_i = [B_i \quad 1 \quad 0 \quad 0 \quad 0]$

where, $x_i \in R^{n_i}$, $u_i \in R^{m_i}$, and $w_i(t) = \Delta P_{Li} \in R^{r_i}$ represent, respectively, the state vector, input vector, and load disturbance in control area i. Matrices A_i, B_i, and D_i represent appropriate system matrices of the control area i.

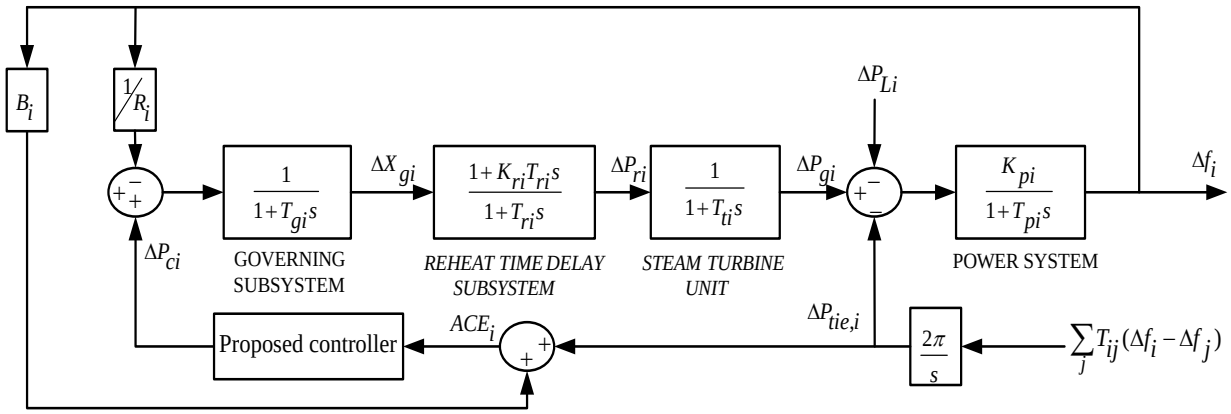

Fig. 1. Block diagram of thermal power plant.

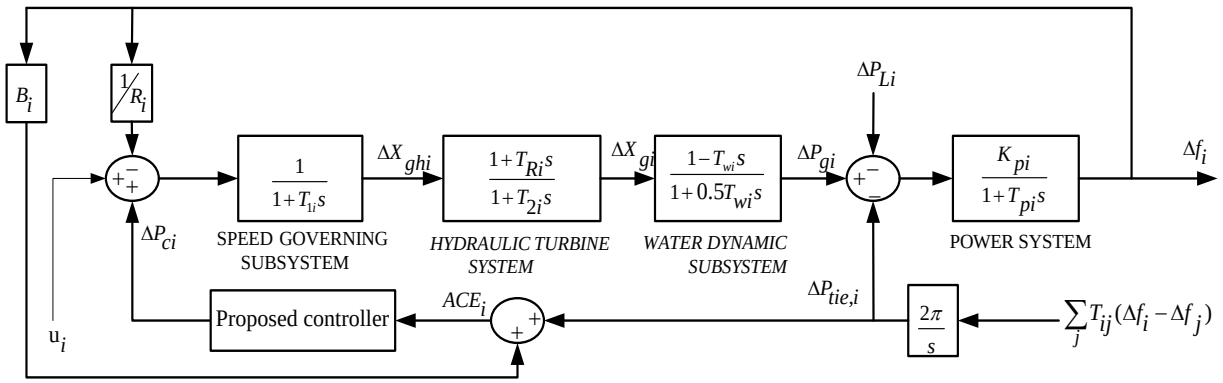

Fig. 2. Block diagram of hydro power plant.

2.2. Renewable energy sources

2.2.1. LFC-based DFIG wind turbine

Currently, the doubly-fed induction generator (DFIG), is widely used in power system in which the power electronic interface controls the rotor currents to generate the variable speed for maximum available energy capture in variable-speed turbines [9]. The variable speed wind energy conversion (WECS) system can extract kinetic energy stored in the mechanical plant of wind turbines which can be utilized to support the frequency regulation. Several frequency control structures like droop control, inertia control, etc. are introduced with these strategy to make DFIGs behave like classical generators.

2.2.1.1. Wind turbine aerodynamic model

This article presents the frequency regulation with variable speed wind turbines employing inertia control strategy and coordinated operation of wind turbine and classical generators. The maximum mechanical power that can be provided from the wind by wind turbine is elaborated by Eq. (11) below [10]:

$$P_{opt} = \frac{1}{2}\rho C_{opt}(\lambda_{opt}, \beta) A V_m^3 \tag{11}$$

where, C_{opt} signifies the optimal power coefficient of the wind turbine modeled as a function of tip speed ratio (λ_{opt}) and pitch angle (β), A is the effective swept area in m^2, V_m is the wind speed in m/s and ρ is the air density in kg/m^3. The optimal power coefficient C_{opt} is given by the following function [10]:

$$C_{opt}(\lambda_{opt}, \beta) = 0.22\left(\frac{116}{\lambda_i} - 0.4\beta - 5\right)e^{-\frac{12.5}{\lambda_i}} \tag{12}$$

$$\frac{1}{\lambda_i} = \frac{1}{\lambda_{opt} + 0.08\beta} - \frac{0.035}{\beta^3 + 1} \tag{13}$$

where the optimal tip speed ratio (λ_{opt}) is given as:

$$\lambda_{opt} = \frac{\omega_{opt} R}{V_m} \tag{14}$$

in which R denotes the blade radius in m and ω_{opt} signifies the optimal wind turbine rotor speed in rad/s .

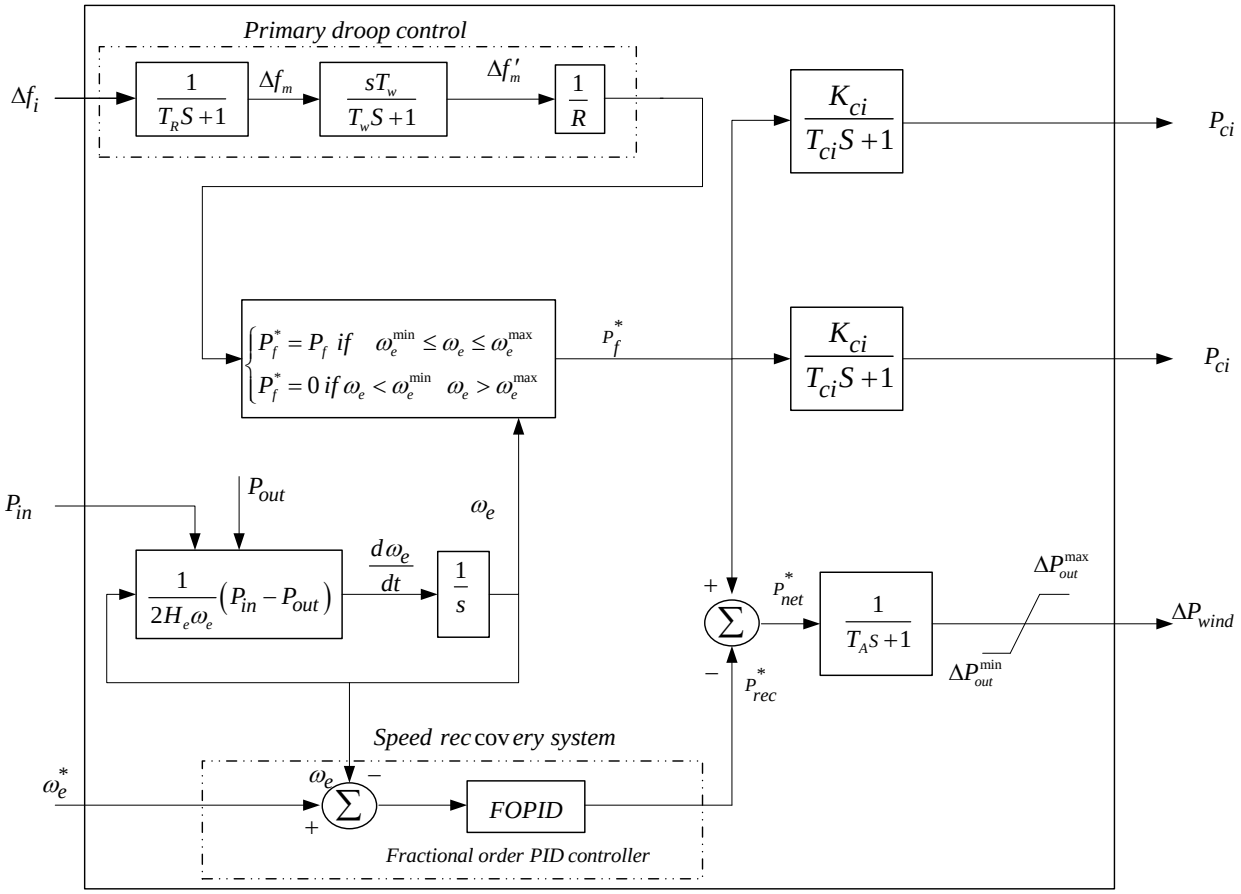

Fig. 3: Block diagram of DFIG based wind turbine model.

2.2.1.2. Strategies employed for frequency regulation of wind turbines

The primary droop and speed recovery strategies are proposed for the frequency regulation of the wind turbine power plant as displayed in Fig. 3. The load perturbations can causes of large frequency oscillations in the power plant, thus in order to handle this effect a droop based control strategy has been employed to assist the primary frequency control for a short period of time after the load change as shown in Fig. 3. In this strategy, the filter is employed in loop to cancel the steady state frequency deviation, and the injected power can be expressed as:

$$P = \frac{1}{R}\Delta f \tag{15}$$

in which P_f signifies the signal given to power electronics scheme and Δf_m denotes the filter frequency error.

Due to an unexpected rate of the stored kinetic energy from the wind turbine generator rotor, the primary droop control strategy gets activated resulting in declining of the rotor speed. To bring the wind turbine generator rotor speed back to its optimal rated value, a fractional order PID (FOPID) controller as presented in Eq. (16) is initiated quickly after the occurrence of load perturbation. This strategy absorbs energy from the network when the frequency error settles down to zero and is relatively slow in comparison with the previous strategy. This strategy avoids the negative influence on the WECS performance.

$$P_{rec} = FOPID = \tilde{K}_p e(t) + \tilde{K}_i \frac{d^{-\eta} e(t)}{dt^{-\eta}} + \tilde{K}_d \frac{d^{\delta} e(t)}{dt^{\delta}} \tag{16}$$

where $e(t) = (\omega_e^* - \omega_e)$, where, $\tilde{K}_p$, $\tilde{K}_i$, $\tilde{K}_d$ are the gains of the controller, η and δ the order of integration and differentiation, respectively.

2.2.2. LFC-based photovoltaic (PV) modeling

Photovoltaic (PV) power system comprises of solar cells it may be arranged in series or in parallel fashion to provide the desired power required by the load demand. The photovoltaic (PV) is modeled and demonstrated as nonlinear voltage-current characteristic relies on the solar radiation as follows [11]:

$$V_{PV} = \left(\frac{N_s \varepsilon Z T_a}{Q}\right) \ln\left(\frac{G I_{ph} N_p - I_{PV} + N_p I_0}{N_p I_0}\right) - I_{PV} R_s \left(\frac{N_s}{N_p}\right) \tag{17}$$

where V_{PV} and I_{PV} represent the PV voltage and current; respectively, T_a is the cell temperature, more detail about the system parameter discussed in [11,12]. The transfer functions of the photovoltaic (PV) system and dc-dc converter with maximum power point tracker algorithm (MPPT) connected to the inverter can be formulated in the following equations [12]:

$$G_1 = \left(\frac{s^2}{s^2 + \omega^2}\right)\left(\frac{V(s^2 + \omega^2)(s^2 + 2\omega^2)}{k s^2 (s^2 + 4\omega^2)}\right)\left(\frac{1 - e^{-sT_s}}{sT_s}\right) \tag{18}$$

$$G_2 = \left(\frac{M_1 / LC}{s^2 + \left(\frac{1}{RC}\right)s + \frac{1}{LC}}\right)\left(\frac{1 - e^{-\frac{sT_s}{2}}}{1 + e^{-\frac{sT_s}{2}}}\right)\left(\frac{M_2}{1 + sT_s}\right) \tag{19}$$

where ω denotes the angular frequency of the grid voltage, R, L and C signify the resistance, inductance and capacitance output of the converter respectively. M_1, M_2 are the dc-dc converter and inverter voltage gain; respectively, T_s denotes the time period.

III. Controller structures

3.1 Fractional order concept

Fractional order (FO) is generally defined by the operator ${}_aD_t^{\alpha}$ which is composed of integer order integral and differential parts, a and t denote the confines of the operation and α is the FO which is a complex number [13].

$${}_aD_t^{\alpha} = \begin{cases} d^{\alpha}/dt^{\alpha}, & \Re(\alpha) > 0 \\ 1, & \Re(\alpha) = 0 \\ \int_a^t (d\tau)^{\alpha}, & \Re(\alpha) < 0 \end{cases} \tag{20}$$

Based on the Riemann-Liouville (R-L) approach, the FO differential and FO integral can be stated as in Eq. (21) and (22) respectively:

$${}_aD_t^{\alpha} f(t) = \frac{1}{\Gamma(n-\alpha)} \frac{d^n}{dt^n} \int_a^t (t-\tau)^{n-\alpha-1} f(\tau) d\tau \tag{21}$$

Where $n-1 > \alpha \geq n$; n is an integer number, and $\Gamma(\cdot)$ signifies the Euler's gamma function.

$${}_aD_t^{\alpha} f(t) = \frac{1}{\Gamma(\alpha)} \int_a^t (t-\tau)^{\alpha-1} f(\tau) d\tau \tag{22}$$

where α $(0 < \alpha < 1)$ in general, the Laplace transformation (LT) of the R-L fractional derivative or integral is modeled by:

$$L\left\{{}_aD_t^{\alpha} f(t)\right\} = s^{\alpha} F(s) - \sum_{k=0}^{n-1} s^k \, {}_aD_t^{\alpha-k-1} f(t)\big|_{t=0} \tag{23}$$

Under zero initial conditions for $n-1 \geq \alpha < n$:

$$L\left\{{}_aD_t^{\pm\alpha} f(t)\right\} = s^{\pm\alpha} F(s) \tag{24}$$

where s signifies the Laplace operator.

3.2. Fractional order PID (FOPID) controller

Fractional order PID (FOPID) or $PI^{\lambda}D^{\mu}$ controller can be formulated as in Eq. (25):

$$u_{FOPID}(t) = K_p e(t) + K_i \frac{d^{-\lambda} e(t)}{dt^{-\lambda}} + K_d \frac{d^{\mu} e(t)}{dt^{\mu}} \tag{25}$$

where, K_p, K_i, K_d represent the gains, λ and μ are the integration and differentiation of fractional order. Hence, the architecture of $PI^{\lambda}D^{\mu}$ controller has five independent knobs to be optimized.

3.3. Fractional order hybrid fuzzy intelligent PID controller design

In this part, the FOF-PID strategy as presented as shown in Fig. 4 which is designed from the fractional order fuzzy PI controller integrated with the fractional order PD controller. In Fig. 4, K_{e1}, K_{e2}, K_{d1}, K_{d2} denote the input factors and K_{pi}, K_{pd} are the output factors. The output signal of the fractional order fuzzy PID (FOF-PID) can be highlighted as in Eq. (26):

$$u_{FOF-PID}(t) = u_{FOF-PI}(t) + u_{FOF-PD}(t) = K_{pi} \frac{d^{-\lambda} u_{FLC-1}(t)}{dt^{-\lambda}} + K_{pd} \, u_{FLC-2}(t) \tag{26}$$

where, $u_{FOF-PI}(t)$ represent the fractional order fuzzy PI controller, $u_{FOF-PD}(t)$ represents the fractional order fuzzy PD controller, and $u_{FOF-PID}(t)$ represents the proposed controller structure output.

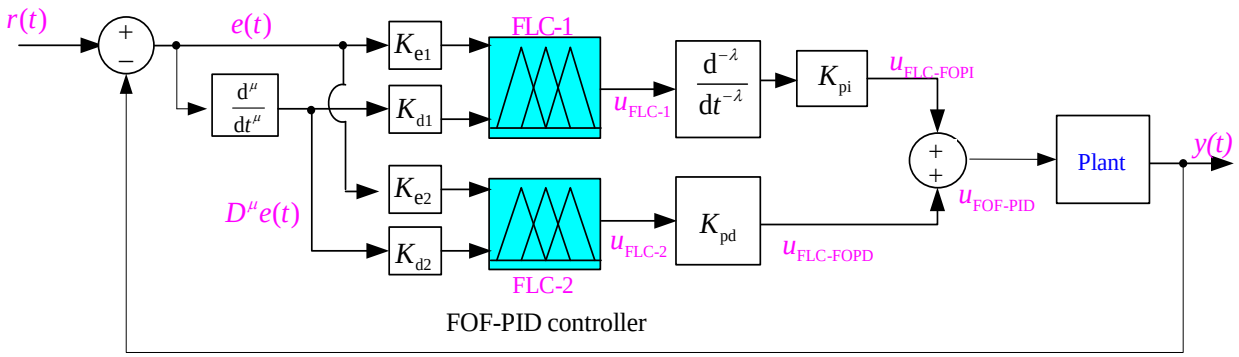

Fig. 4: Fraction order hybrid fuzzy PID controller architecture.

The error $(e(t))$ and its fractional derivative $(D^{\mu}e(t))$ are selected as input variables of the proposed controllers, and $(u_{FLC-1}), (u_{FLC-2})$ is selected as the output variables of the fuzzy controller. These variables are fuzzified into 7 triangular membership functions which are characterized by linguistic variables, and then the rule base associated with the fuzzy controller are furnished in Table 1. Finally, the output of the proposed controller (u_{FOiPID_FOFPID}) is subjected to the interconnected multi-source power system. In doing so, the associated gains and the scaling parameters are optimized by employing hFA-PSO algorithm.

Table 1: Fuzzy rule base.

$\frac{d^{\mu}e(t)}{dt^{\mu}}$ \ $e(t)$	NL	NM	NS	Z	PS	PM	PL
PL	Z	PS	PM	PL	PL	PL	PL
PM	NS	Z	PS	PM	PL	PL	PL
PS	NM	NS	Z	PS	PM	PL	PL
Z	NL	NM	NS	Z	PS	PM	PL
NS	NL	NL	NM	NS	Z	PS	PM
NM	NL	NL	NL	NM	NS	Z	PS
NL	NL	NL	NL	NL	NM	NS	Z

IV. A hybrid firefly and particle swarm optimization algorithm:

4.1. Firefly optimization algorithm:

Firefly algorithm (FA) is one of the most lately developed swarm intelligence technique, which introduced by Yang [14]. The technique is motivated by flashing characteristic of the fireflies. Flashing light fashioned by the firefly in the bio-inspired meta-heuristics process is the motive behind the development of the algorithm. This flashing light gives out courtship signals for mating. Modern research demonstrates that the FA is very efficient and may provide better results than other similar approaches [15].

For proper designed of firefly algorithm (FA), a number of important issues such as the change in light intensity, the attractiveness of fireflies, number of population and generation are to be appropriately chosen [15]. While the brightness of fireflies depends on the function to be tuned, their attractiveness is adjusted by its light intensity. Light intensity $I_{(r)}$ relies on distance as presented below:

$$I_{(r)} = I_0 e^{-\gamma r} \tag{27}$$

where, I_0 signifies the intensity of flight at original, and γ represent the light absorption factor. As a firefly's attractiveness is proportional to the light intensity seen by neighboring fireflies, the attractiveness β of a firefly is derived as:

$$\beta = \beta_0 e^{-\gamma r^2} \tag{28}$$

in which β_0 denotes the attractiveness at $r = 0$.

The distance between any two fireflies s_i and s_j is modeled by Euclidean distance as:

$$r_{ij} = \left\| x_i - x_j \right\| = \sqrt{\sum_{k=1}^{k=n} (x_{i,k} - x_{j,k})^2} \tag{29}$$

where n signifies the dimensionality of the issue. The movements of fireflies comprise of three terms: the present location of ith firefly, attraction to another more attractive firefly, and stochastic walk that comprises of a randomization parameter Ξ and the stochastic produced number $\Upsilon_i \in [0;\ 1]$. The movement is derived as:

$$x_i = x_i + \beta_0 e^{-\gamma r_{ij}^2}(x_i - x_j) + \Xi \Upsilon_i \tag{30}$$

The flowchart of firefly is shown in Fig. 5.

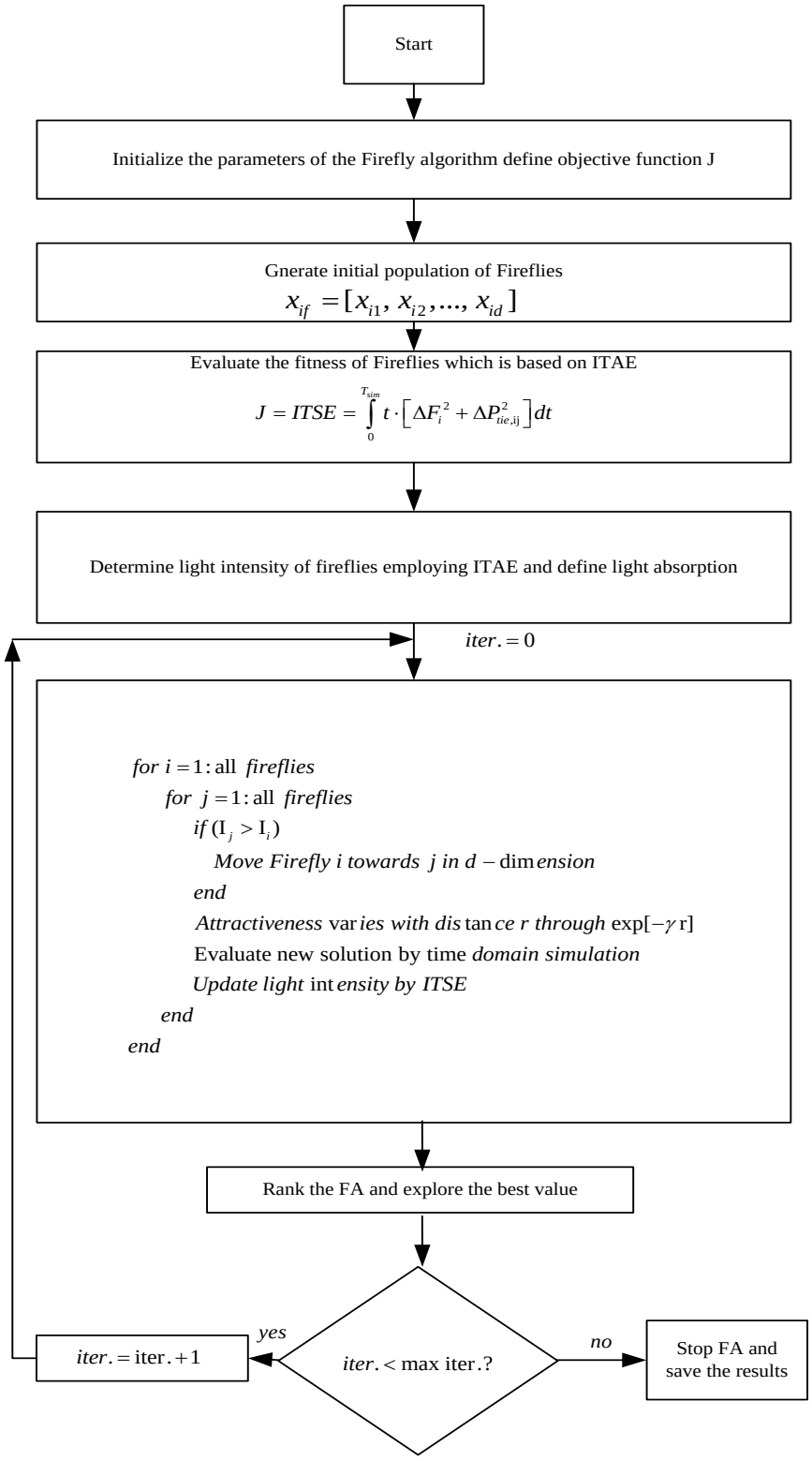

Fig. 5: Flowchart of the FA algorithm.

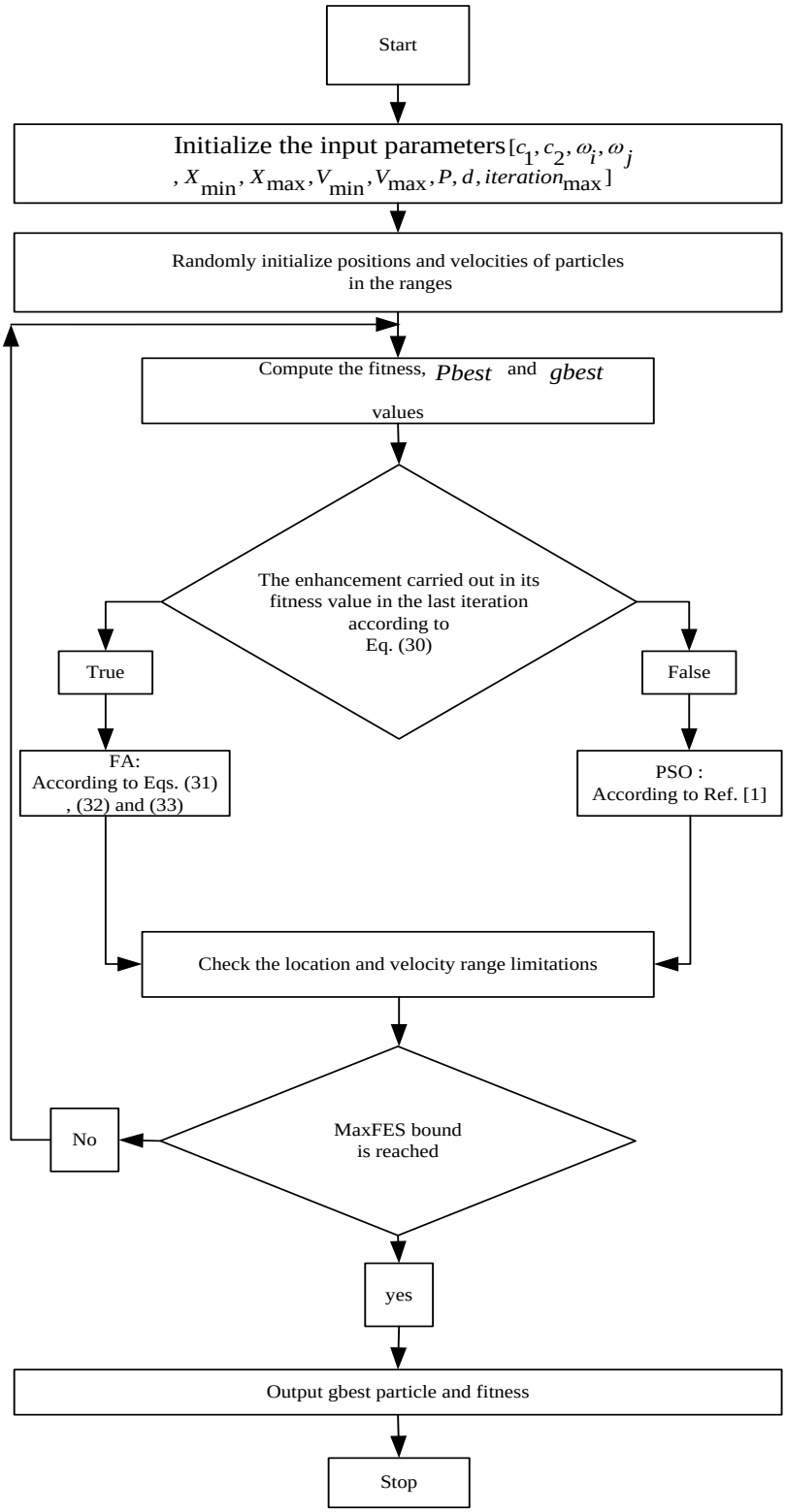

Fig. 6: Flowchart of the proposed hFA-PSO algorithm.

4.2. Proposed a hybrid firefly and particle swarm optimization (hFA-PSO) algorithm:

Realizing a reliable success in assessing a limited number of functions is the main objective of the suggested hFA-PSO algorithm. Therefore, the speed of convergence is significant in the early phase of iterations. PSO technique has faster convergence capability rather than several other techniques in certain problems, as introduced in [1]. This fast convergence ability in the PSO local search phase, decreases and decelerates down especially when searching in the solution space near to a global optimal solution. The Equilibrium between exploration and exploitation in the PSO technique can be efficiently handled by

employing control parameters of the PSO: inertia weight (ω), acceleration coefficients (c_1, c_2). Velocity of a particle (v) can be computed by utilizing these control parameters. The value of particle velocity is important in local search, but calculating the appropriate velocity can be a defying task through local search, as incorrect values can cause particles to fluctuate around optimal solution. These fluctuation cause some delays in the whole optimization issue. As a result of this problem, velocity can be ignored in exploitation phases. In the other hand, FA technique does not have a velocity (v) characteristic [16]. In addition, there have no parameters in FA technique to utilize preceding best location of each firefly. Therefore, fireflies can move regardless of their preceding best locations.

In this article, an optimization technique that combines search capability of FA and PSO algorithms has been proposed. Thus, the equilibrium between exploration and exploitation is intended to establish and it benefits supports of both algorithms. Since in fireflies have not velocity (v) and personal best position ($pbest$) memories in comparison to particles. In the suggested hybrid combination of two techniques: PSO is generally employed in the global search, because it provides fast convergence in exploration as well as FA is used in local search, because it provides well-tuning in exploitation. The flowchart of the proposed hybrid firefly and particle swarm optimization (hFA-PSO) algorithm is highlighted in Fig. 6. The input parameters that are employed by both algorithms in the proposed algorithm are inserted and the uniform particle vectors are stochastically prepared in the pre-defined search and velocity ranges. the global ($gbest$) and personal best ($pbest$) particles are computed and assigned. In the subsequent comparing phase, it is compared that if particle has an enhancement in its fitness value in the previous iteration according to Eq. (31). Then present location is reserved in a temp variable (X_{i-temp}) and the new location and velocity are computed according to Eqs. (32) and (33).

$$f(i,t) = \begin{cases} T, if \ \ fitness\,(particle_i^t) \le gbest^{t-1} \\ F, if \ \ fitness\,(particle_i^t) > gbest^{t-1} \end{cases} \tag{31}$$

where, T mean true, F mean false

$$X_i(t+1) = X_i(t) + \beta_0 e^{-\gamma r_{ij}^2}\left(X_i(t) - gbest^{t-1}\right) + \Xi \Upsilon_i \tag{32}$$

$$V_i(t+1) = X_i(t+1) - X_{i-temp} \tag{33}$$

According to above, if a particle has an improved or equal fitness value than preceding global best, it is expected that local search starts and particle is controlled by FA technique, otherwise particle will be controlled by PSO technique and PSO continues its standard procedures with this particle. In the following subsequent comparing phase, fitness function assessments and range limitations are checked for all particles and fireflies. If the maximum repetition limit is reached, hybrid algorithm will be ended, whereas $gbest$ and its fitness value will be specified as output of suggested hybrid algorithm. The pseudo code of the suggested hFA-PSO technique is well-demonstrated in algorithm 1. In an evolutionary calculating the maximum number of fitness function evaluation (MaxFES) is a popular termination benchmark that allowed the maximum computation of objective functions. The inertia weight (ω) parameter helps to equilibrium between exploration and exploitation in PSO technique, which can be derived it according to Eq. (34). The Maximum and minimum velocities of a particle ($V_{\max}$, $V_{\min}$) are utilized to confine the next distance in a direction.

$$\omega = \omega_i - ((\omega_i - \omega_f) / iteration_{\max}) * iteration \tag{34}$$

To compensate the imbalance between generation and load demand of a power plant, the area control error (ACE) should be derived to zero by appropriate adjustment of the regulator parameters. In a well-restructured LFC, the system performance in the transient state should basically be at a satisfactory level of responsiveness, fast, damped oscillations, and simultaneously the dynamic stability of the plant guaranteed. Thus, to achieve the design objectives of power plants by inspired algorithms, a suitable objective function it essentials to be selected so that the desired outcomes of the transient response in terms of settling time, rise time, peak overshoot and steady-state error be obtained. In this article, PSO, FA and hybrid firefly-based particle swarm optimization (hFA-PSO) algorithm are employed in this article to optimize the parameter of proposed controller. For which the integral of time multiplied squared error (ITSE) as presented in Eq. (35) is designated as the performance index to assess the performance of the multi-area power system.

$$J = ITSE = \int_0^{T_{sim}} t \cdot \left[\Delta F_i^{\,2} + \Delta P_{tie,ij}^{\,2}\right] dt \tag{35}$$

where, T_{sim} signifies the simulation time. In this study, the minimum and maximum parameters for the proposed controller are designated in the range [0 3].

Table 2: System parameters

Hydro-thermal parameters					
Parameter	Unit	Value	Parameter	Unit	Value
T_{pi}	[s]	20	T_{2i}	[s]	10
T_t	[s]	0.3	T_{Ri}	[s]	0.513
T_{r1}	[s]	10	T_{1i}	[s]	48.7
K_{r1}	[Hz/ p.u.MW]	0.5	T_{wi}	[s]	1.0
T_g	[s]	0.08	B_i	[p.u.MW/ Hz]	0.425
R	[Hz/ p.u.MW]	2.4	T_{ij}	[p.u.MW]	0.08674
B	[p.u.MW/ Hz]	0.425	a_{ij}		1.0
	Notice: $i = 1, 2, 3$ *and* 4.				

V. Simulation results and discussion

5. Simulation results

To validate the effectiveness of the proposed LFC of the interconnected power system in the presence of RESs two cases are studied; the first one comprises from thermal and photovoltaic interconnected power plants while the second case comprises four-area, every area have multi-source power plants namely: thermal, hydro, PV and wind turbine generating units. The corresponding parameters for the proposed system is furnished in Table 2. The modeling of the systems under study are carried out using MATLAB/SIMULINK platform. The controller gains of the simulations procedure are regulated via PSO, CPSO, FA and hybrid firefly-particle swarm optimization (hFA-PSO) algorithms. Maximum iteration size is designated equal in entirely experiments, while the controller parameters of the algorithms are selected as: In PSO algorithm: $c_1 = c_2 = 1.759$, $\omega_i = 0.85$, $\omega_f = 0.55$ are used. In FA algorithms, $\Xi = 0.43$, $\beta_0 = 1.95$, $\gamma = 0.75$. The simulation procedure of the proposed strategy can be divided into following subsections:

1- Two-area interconnected power systems,
2- Multi-area multi-source interconnected systems:
   - Case 1: Performance analysis considering 10% step load perturbation,
   - Case 2: Sensitivity analysis,
   - Case 3: Performance analysis under step load change with wind turbine and PV system.

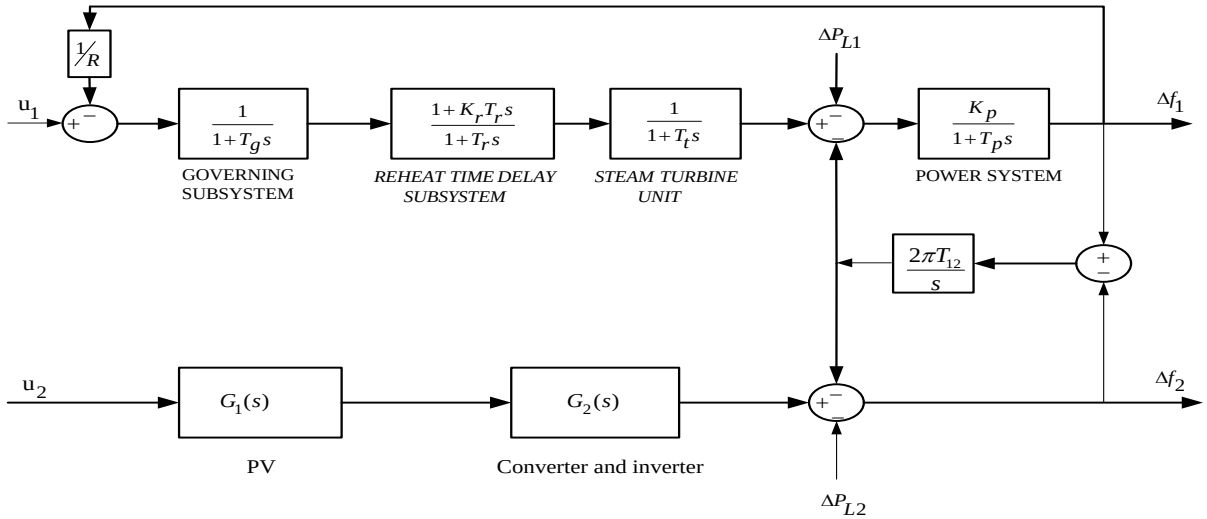

Fig. 7. Block diagram of Thermal/PV interconnected power plant.

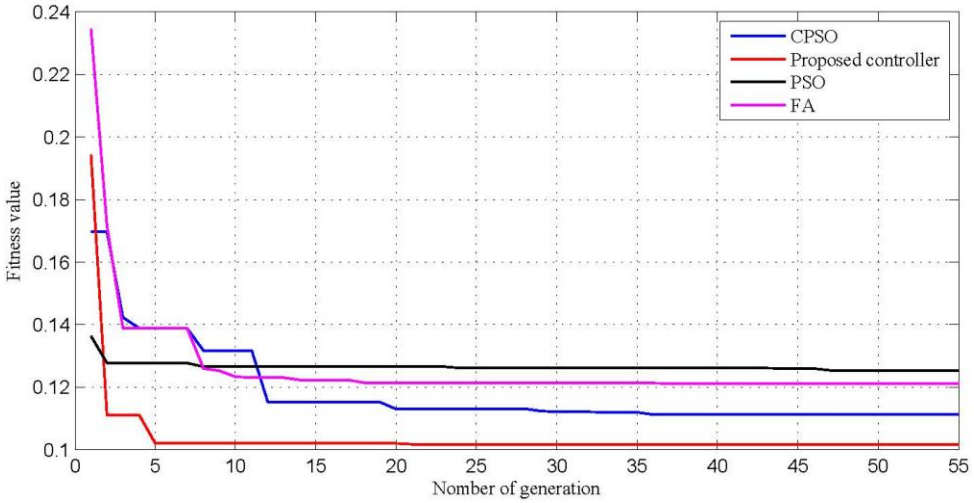

Fig. 8: Convergence characteristics.

Table 3: Controlling parameters of CPSO, PSO, and FA and the proposed hFA-PSO optimized FOF-PID controller.

Controllers	Controller gains							
	K_{e1}	K_{e2}	K_{d1}	K_{d2}	K_{pi}	K_{pd}	λ	μ
FOF-PID optimized via FA	-2.056	-1.765	1.876	-0.654	1.876	1.765	0.765	0.987
FOF-PID optimized via PSO	1.654	1.875	-1.765	0.543	-1.654	-1.765	0.997	0.8765
FOF-PID optimized via CPSO	-0.678	-1.005	-1.876	-1.654	-1.123	1.765	0.654	0.876
Proposed controller	1.097	-2.765	2.065	2.765	-3.432	-1.875	0.543	0.998

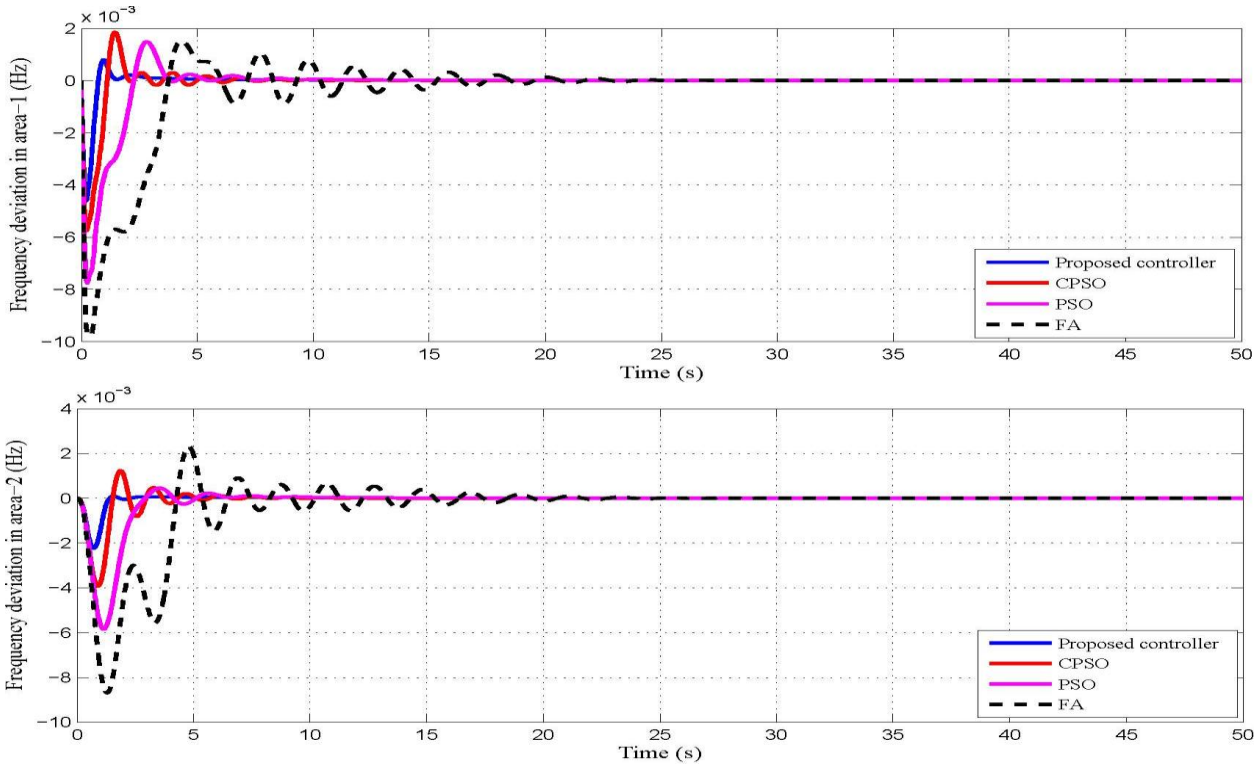

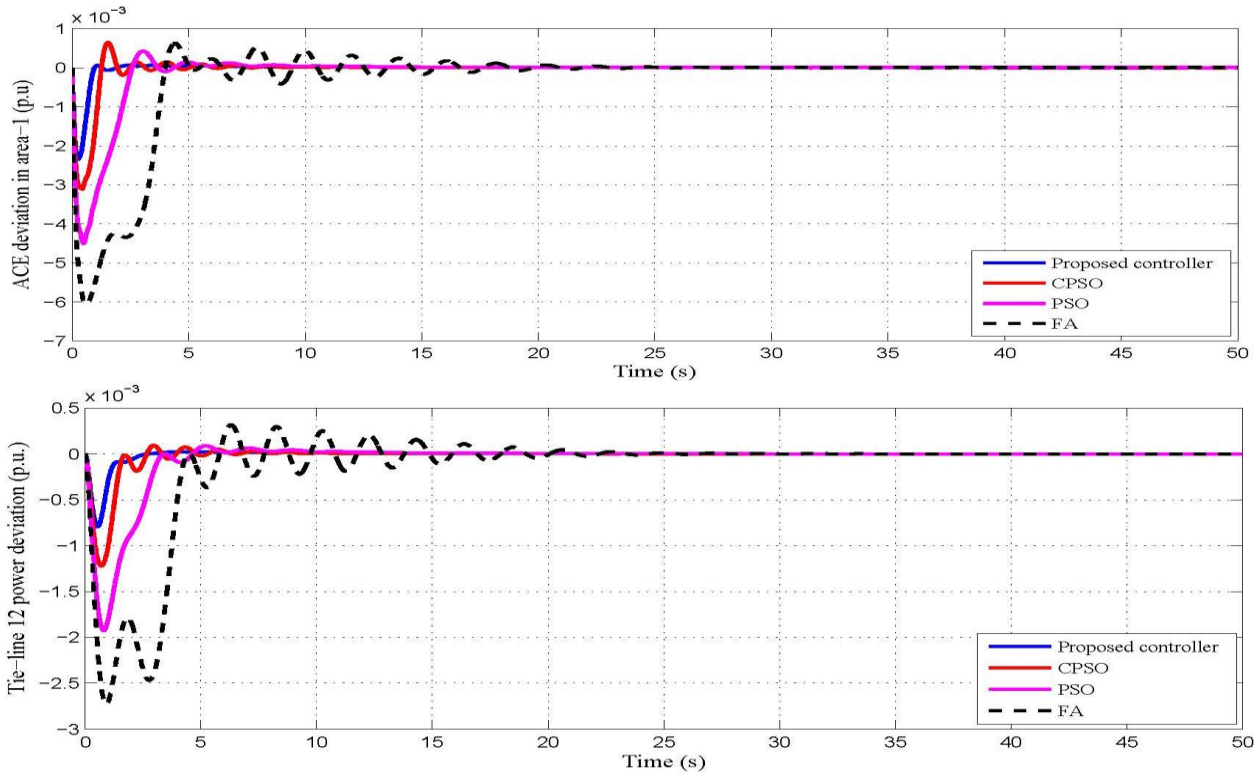

Fig. 9. Time responses of the frequency, area control error and tie-line power deviations for the plant after 10% step load perturbation.

5.1. Two-area interconnected power system:

In this scenario two-area interconnected power plant as displayed in Fig. 7 has been considered for study; where area-1 comprises reheat thermal power generation system and area-2 comprises photovoltaic (PV) system. The suggested system incorporated with 10% step load perturbation in area-1, while the system parameters of each unit are furnished in Table 2. The obtained results of the proposed strategy are compared with those attained by particle swarm optimization (PSO), CPSO, and firefly algorithm (FA). The optimal gains of FOF-PID controller, obtained via a hybrid hFA-PSO optimizer compared to PSO, CPSO, and FA results are tabulated in Table 3. Fig. 8 shows the convergence response of hFA-PSO compared to CPSO, PSO, and FA algorithms for the best objective function. It is clear that the convergence of hFA-PSO is faster and the objective function of the hFA-PSO decreases over the generations comparing to CPSO, PSO, and FA algorithms. The hFF-PSO optimizer succeeded in achieving the optimum solution after 7.192 s while the CPSO consumes 21.7 s, PSO consumes 21.7 s, FA consumes 21.7 s to get the optimum solution. One can conclude that, the obtained results via the proposed strategy are the best with short time convergence compared to the others. Fig. 9 and Table 4 shows the performance specifications (settling time, over shoot, under shoot, and ITSE) of frequency error, area control error and tie-line power deviation obtained by the proposed FOF-PID controller in comparison with those obtained via CPSO, PSO, and FA algorithms. It is clear that, the specifications obtained via hFA-PSO optimized FOF-PID controller are the best compared to CPSO, PSO, and FA approaches, the proposed strategy is superior in obtaining the steady state performance of the proposed interconnected power systems.

Table 4: The optimal results obtained by hFA-PSO optimized FOF-PID compared with CPSO, PSO, and FA.

Controller	Settling time (s)				Peak overshoot				Peak undershoot (-ve)				ITSE
	Δf_1	Δf_2	ACE_1	$\Delta P_{tie,12}$	Δf_1	Δf_2	ACE_1	$\Delta P_{tie,12}$	Δf_1	Δf_2	ACE_1	$\Delta P_{tie,12}$	Value
FOF-PID optimized via FA	4.61	7.01	9.13	10.01	0.0015	0.0023	0.0006	0.0003	0.0097	0.0087	0.0059	0.0027	0.0267
FOF-PID optimized via PSO	3.10	2.35	2.44	2.94	0.0014	0.0005	0.0004	0.00002	0.0076	0.0058	0.0044	0.0018	0.0131
FOF-PID optimized via CPSO	1.72	1.45	1.56	1.44	0.0018	0.0012	0.0006	0.00001	0.0059	0.0037	0.0030	0.0012	0.0081
Proposed controller	0.73	1.15	0.84	1.06	0.0007	0.0	0.0	0.0	0.0044	0.0021	0.0021	0.0008	0.0048

5.2. Multi-area multi-source interconnected systems:

5.2.1. Case I: Performance analysis under step load perturbation:

In this case a four-area interconnected power system as highlighted in Fig. 10 have being proposed for study; where every control area has thermal/hydro power plants. The system is incorporated with the proposed FOF-

PID controller optimized via hFA-PSO technique, under 10% step load perturbation in area-1. Optimal setting of the controller parameters are optimized via CPSO, PSO, FA, hFA-PSO techniques and listed in Table 5. The effectiveness of the suggested approach is compared with CPSO, PSO and FA algorithms. Fig. 11 show the frequency errors, area control errors and tie-line power deviations of the proposed system. The dynamic specifications of the plant in terms of ITSE, settling time, and peak overshoot/undershoot are gathered in Tables 6 and 7. It is noted from Tables 6 that the hFA-PSO optimized FOF-PID controller provides a smaller objective function (ITSE = 0.0228) than CPSO optimized FOF-PID controller (ITSE = 0.0258), PSO optimized FOF-PID controller (ITSE = 0.0289), FA optimized FOF-PID controller (ITSE = 0.0332). It can be summarized from Tables 6, 7 and Fig. 11, that the performance oscillations are properly settled down to the steady value in a small time by the proposed control technique. Thus the desirable dynamic stability for sudden change in the load demand is accomplished by FOF-PID controller optimized via hFA-PSO algorithm and the proposed technique is outperforms the other techniques.

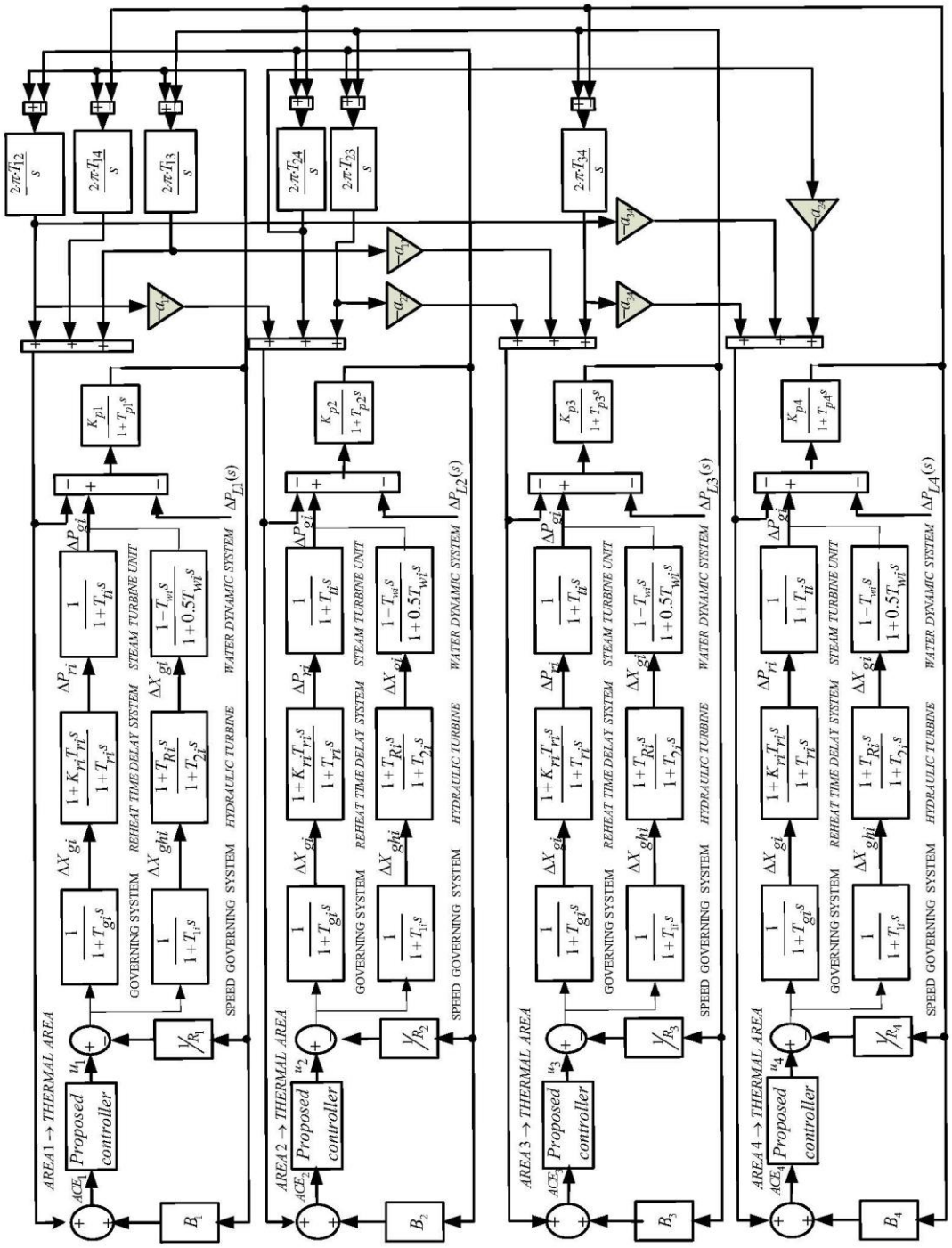

Fig. 10: Four area power system under investigation for case I.

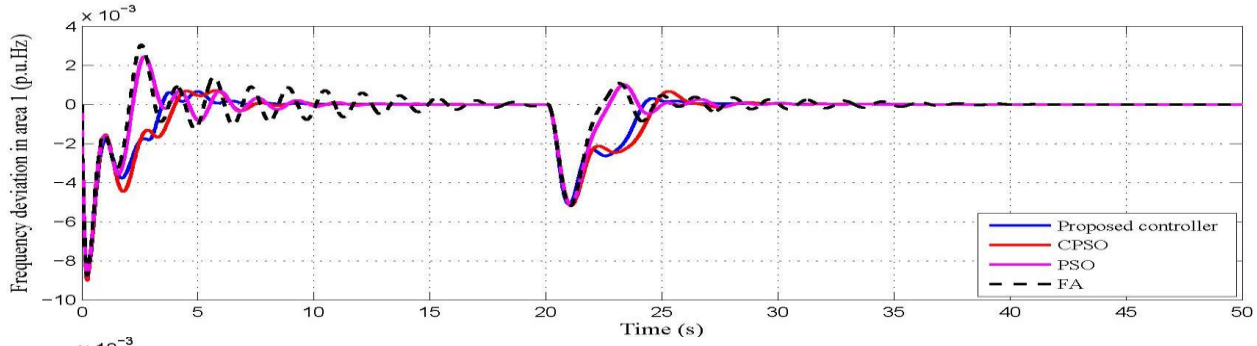
x 10^-3
Frequency deviation in area 1 (p.u.Hz)
Time (s)
Proposed controller
CPSO
PSO
FA

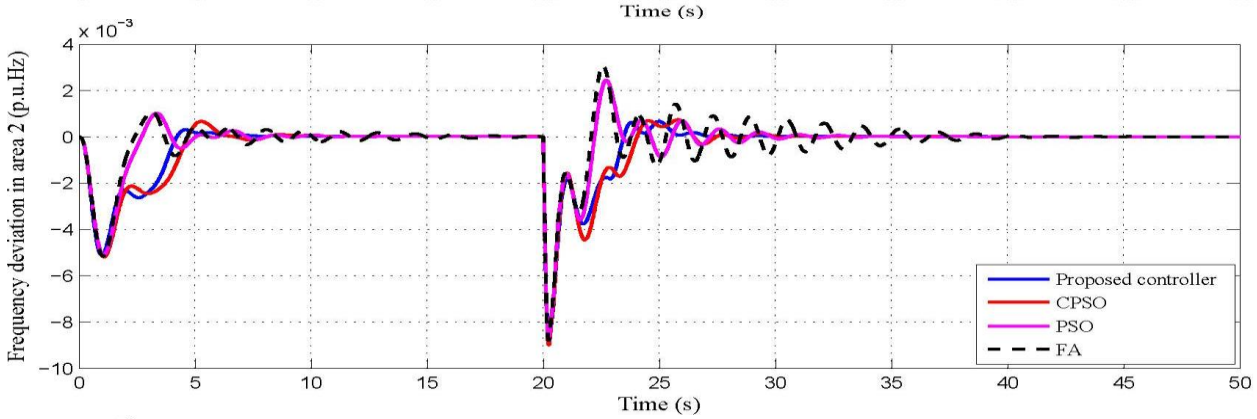
x 10^-3
Frequency deviation in area 2 (p.u.Hz)
Time (s)
Proposed controller
CPSO
PSO
FA

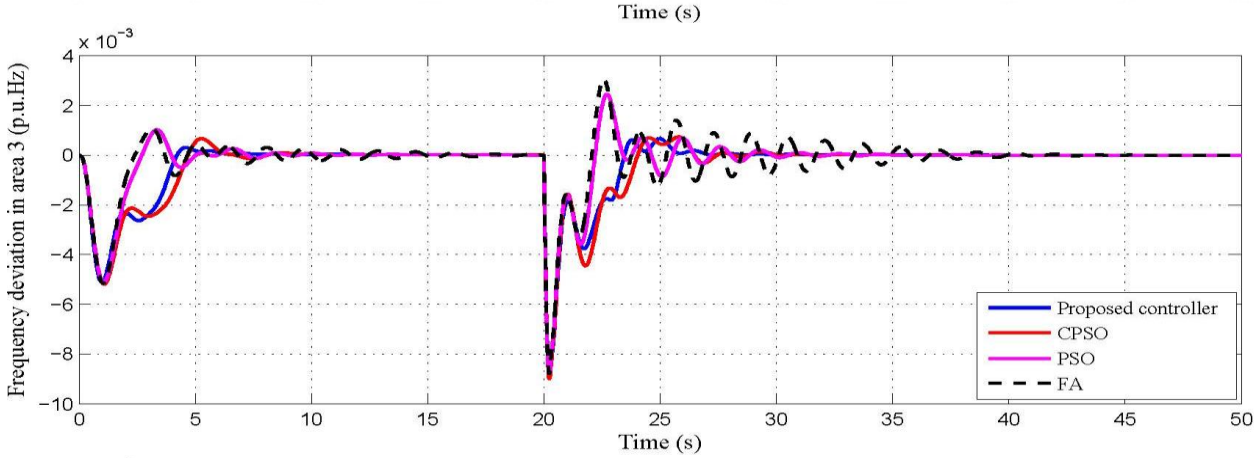
x 10^-3
Frequency deviation in area 3 (p.u.Hz)
Time (s)
Proposed controller
CPSO
PSO
FA

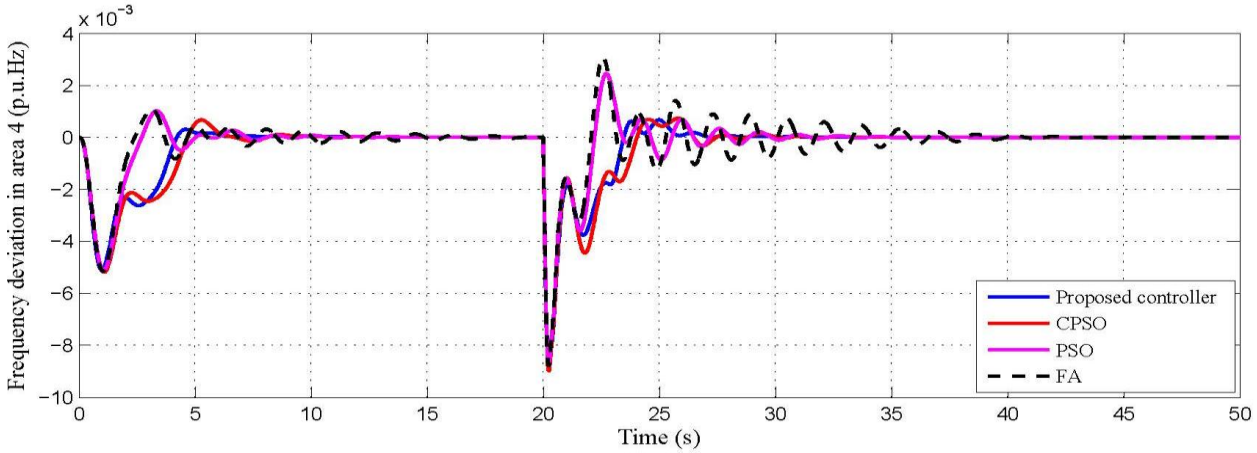
x 10^-3
Frequency deviation in area 4 (p.u.Hz)
Time (s)
Proposed controller
CPSO
PSO
FA

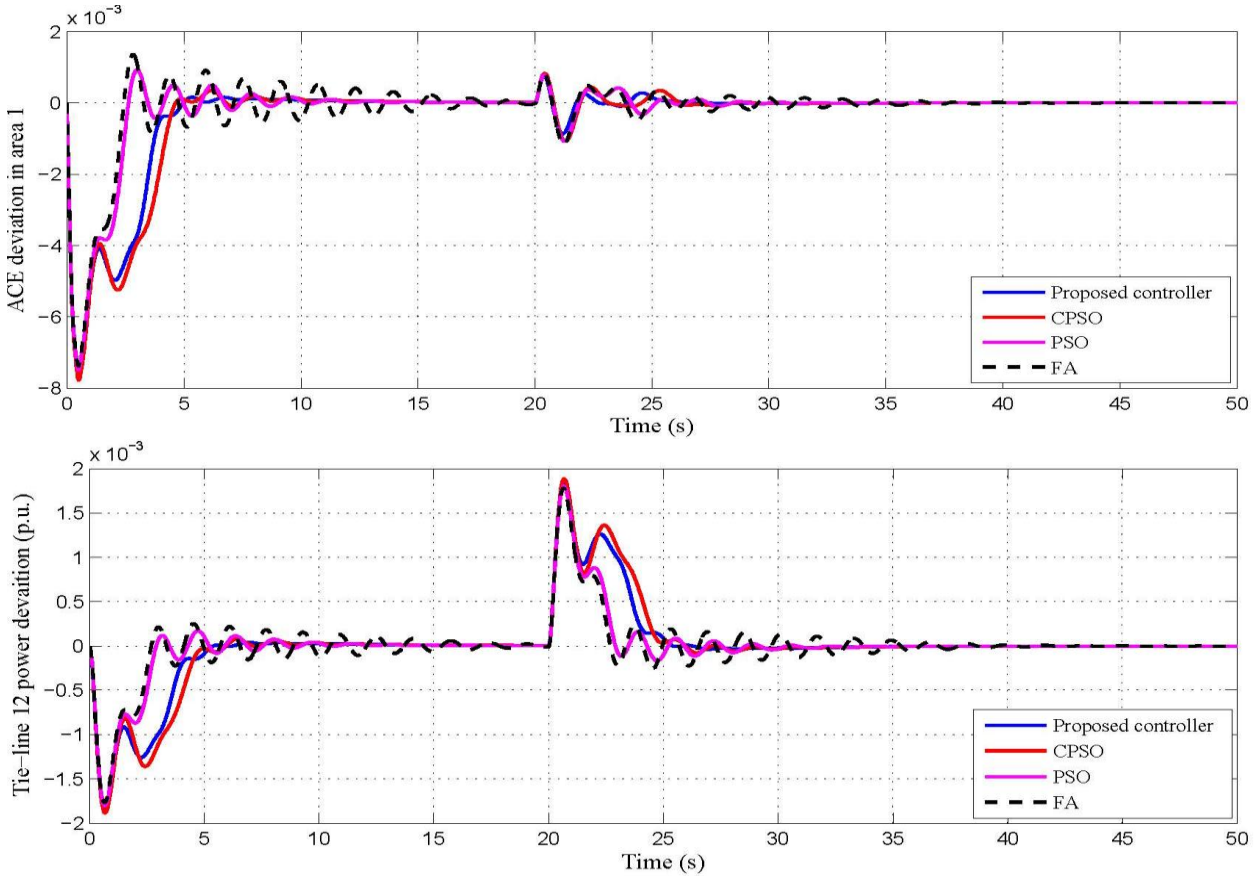

Fig. 11. Comparative dynamic performances of the plant in term of frequency, area control error, and tie-line power deviations for case I.

Table 5: Optimized controllers parameters for case I.

Controllers	Controller gains							
	K_{e1}	K_{e2}	K_{d1}	K_{d2}	K_{pi}	K_{pd}	λ	μ
FOF-PID optimized via FA	0.235	2.345	0.365	-0.067	-0.543	-2.765	0.765	0.876
FOF-PID optimized via PSO	0.363	-0.254	-2.872	0.187	0.654	0.564	0.675	0.763
FOF-PID optimized via CPSO	-1.548	1.654	1.653	-0.654	-2.765	-0.6538	0.876	0.762
Proposed controller	1.064	-0.987	-3.570	0.563	1.654	2.765	0.905	0.998

Table 6: Comparative analysis of the system in terms of ITSE and settling time for case I.

Controller	ITSE	Settling time (s)					
	Value	Δf_1	Δf_2	Δf_3	Δf_4	$\Delta P_{tie,12}$	ACE_1
FOF-PID optimized via FA	0.0332	8.99	4.27	4.27	4.27	6.19	10.54
FOF-PID optimized via PSO	0.0289	5.11	4.18	4.18	4.18	4.92	6.42
FOF-PID optimized via CPSO	0.0258	3.76	4.15	4.15	4.15	4.47	4.44
Proposed controller	0.0228	3.29	3.72	3.72	3.72	3.84	3.79

Table 7: Comparative analysis of the system in terms of peak over/undershoot for case I.

Controller	Peak undershoot (-ve)						Peak overshoot					
	Δf_1	Δf_2	Δf_3	Δf_4	$\Delta P_{tie,12}$	ACE_1	Δf_1	Δf_2	Δf_3	Δf_4	$\Delta P_{tie,12}$	ACE_1
FOF-PID optimized via FA	0.0086	0.0052	0.0052	0.0052	0.0018	0.0076	0.0031	0.0011	0.0011	0.0011	0.0003	0.0013
FOF-PID optimized via PSO	0.0079	0.0051	0.0051	0.0051	0.0017	0.0073	0.0025	0.0010	0.0010	0.0010	0.0002	0.0009
FOF-PID optimized via CPSO	0.0085	0.0051	0.0051	0.0051	0.0018	0.0077	0.0007	0.0006	0.0006	0.0006	0.0001	0.0003
Proposed controller	0.0073	0.0050	0.0050	0.0050	0.0016	0.0072	0.0005	0.0002	0.0002	0.0002	0.0	0.0001

Table 8: Sensitivity analysis of the plant with the proposed FOF-PID optimized via hFA-PSO.

Parameter variation	% Change	ITSE	Settling time (Sec) for 5% band						Peak undershoot (−ve)					
		Value	Δf_1	Δf_2	Δf_3	Δf_4	$\Delta P_{tie,12}$	ACE_1	Δf_1	Δf_2	Δf_3	Δf_4	$\Delta P_{tie,12}$	ACE_1
Nominal	No change	0.0228	3.29	3.72	3.72	3.72	3.84	3.79	0.0073	0.0050	0.0050	0.0050	0.0016	0.0072
Loading condition	+50	0.0467	4.89	5.32	5.32	5.32	5.73	5.94	0.0123	0.0102	0.0102	0.0102	0.0045	0.0131
	+25	0.0332	3.56	3.89	3.89	3.89	4.56	3.89	0.0100	0.0092	0.0092	0.0092	0.0032	0.0101
	-25	0.0201	2.92	3.43	3.43	3.43	3.52	3.23	0.0056	0.0042	0.0042	0.0042	0.0010	0.0053
	-50	0.0200	2.67	3.32	3.31	3.31	3.32	3.01	0.0050	0.0040	0.0040	0.0040	0.0098	0.0050
T_g	+50	0.0230	3.3	3.74	3.74	3.74	3.85	3.81	0.0076	0.0054	0.0054	0.0054	0.0018	0.0075
	+25	0.0229	3.29	3.73	3.73	3.73	3.85	3.80	0.0074	0.0052	0.0052	0.0052	0.0017	0.0074
	-25	0.0227	3.28	3.71	3.71	3.71	3.82	3.77	0.0072	0.0050	0.0050	0.0050	0.0015	0.0071
	-50	0.0226	3.27	3.70	3.70	3.70	3.82	3.76	0.0071	0.0049	0.0049	0.0049	0.0014	0.0070
T_r	+50	0.0232	3.34	3.92	3.92	3.92	3.91	3.81	0.0081	0.0054	0.0054	0.0054	0.0018	0.0076
	+25	0.0231	3.32	3.75	3.75	3.75	3.88	3.80	0.0079	0.0052	0.0052	0.0052	0.0018	0.0076
	-25	0.0226	3.27	3.70	3.70	3.70	3.81	3.76	0.0071	0.0048	0.0048	0.0048	0.0014	0.0070
	-50	0.0224	3.25	3.68	3.68	3.68	3.80	3.74	0.0070	0.0046	0.0046	0.0046	0.0013	0.0068
T_{12}	+50	0.0222	3.23	3.64	3.64	3.64	3.77	3.74	0.0067	0.0046	0.0046	0.0046	0.0012	0.0069
	+25	0.0226	3.27	3.71	3.71	3.71	3.82	3.77	0.0071	0.0049	0.0049	0.0049	0.0015	0.0070
	-25	0.0231	3.33	3.75	3.75	3.75	3.89	3.81	0.0082	0.0056	0.0056	0.0056	0.0021	0.0078
	-50	0.0235	3.36	3.79	3.79	3.79	3.92	3.84	0.0086	0.0059	0.0059	0.0059	0.0025	0.0081

5.2.2. Case II: Sensitivity analysis.

The performance evaluating of the interconnected complex power plant against wide variations in system parameters is a typical measure to appraise the robustness of the close-loop system. Generally, the robust structure designed for LFC mechanism must have sufficient ability versus the plant uncertainties to preserve the frequency and transmission-line power oscillations in a desired level of deviations. Therefore, to validate the advantages of the suggested FOF-PID controller optimized via hFA-PSO algorithm versus robustness analysis, we take the same the plant as in case I with the same regulated gains (Table 5). Then, the interconnected complex power plant is examined by changing the operating load condition and some critical parameters of the plant such as T_g, T_r, and T_{12} in the range of ±40% from the nominal values. The lowest ITSE values, settling time and peak undershoot of the proposed plant under the aforesaid uncertainties are furnished in Table 8 . It is inspected from Table 8 that the impact of uncertainties on fitness value, settling time and peak undershoot derived by the hFA-PSO based FOF-PID controller in nominal condition is insignificant. Having knowledge of the above analysis, it can be inferred that the suggested FOF-PID controller optimized via hFA-PSO algorithm are quite robust and perform satisfactory results even against the uncertainties.

5.2.3. Case III: Performance analysis under step load change with RESs.

For the time being, most of power plants have more than one generation utility as hydro, thermal, gas, nuclear, wind, photovoltaic. Therefore, to deal with real power plant model, different generation utility multi-interconnected power plants are studied. In order to assess the reliability of the proposed load frequency controller, a four-area interconnected power system have being considered; where every control area have multi-source generation units namely: Thermal, hydro, photovoltaic and wind power generations have being considered in this work. The data of wind turbine system is taken from [17], the data of PV system is taken from [11]. The interconnected power system incorporated with the proposed controller under step load perturbation $\Delta P_{L1} = 0.01$ in area-1 and the optimal gains of the controllers are furnished in Table 9. The obtained results of Δf_1, Δf_2, Δf_3, Δf_4, $\Delta P_{tie,12}$ and ACE_1 are shown in Figs. 12 in comparison with hFA-PSO, CPSO, PSO, and FA optimized FOF-PID controller. From the simulation results one can get that, the suggested FOF-PID controller optimized via hFA-PSO succeeded in obtaining the best performances than those obtained via CPSO, PSO and FA. The performance specifications of the frequency, area control error and tie line power errors are presented in Tables 10 and 11 in comparison with hFA-PSO, CPSO, PSO, and FA optimized FOF-PID controller. From the Table 10, it can observe that the proposed controller optimized via hFA-PSO gives the optimal ITSE function of 0.0059, while CPSO gives ITSE index of 0.0106, PSO gives ITSE index of 0.0088, FA gives ITSE index of 0.0217. Finally, one can get that the proposed controller regulated via hFA-PSO succeeded in obtaining zero frequency and tie line power deviations for interconnected multi-utilities system subjected to load perturbation.

Table 9: Optimized controllers parameters for case 4.

Controllers	Controller gains							
	K_{e1}	K_{e2}	K_{d1}	K_{d2}	K_{pi}	K_{pd}	λ	μ
FOF-PID optimized via FA	-2.654	1.764	1.564	-1.452	-1.531	1.543	0.654	0.915
FOF-PID optimized via PSO	4.763	-2.043	-0.654	1.760	0.654	-1.954	0.153	0.786
FOF-PID optimized via CPSO	-2.065	1.764	1.543	-0.754	-0.431	0.546	0.653	0.876
Proposed controller	0.572	-2.785	-1.065	0.543	0.542	-0.342	0.543	0.987

Table 10: Comparative analysis of the system in terms of ITSE and settling time case 4

Controller	ITSE	Settling time (s)					
	Value	Δf_1	Δf_2	Δf_3	Δf_4	$\Delta P_{tie,12}$	ACE_1
FOF-PID optimized via FA	0.0217	9.02	8.84	8.84	8.84	15.41	15.19
FOF-PID optimized via PSO	0.0088	3.58	2.54	2.54	2.54	5.76	5.56
FOF-PID optimized via CPSO	0.0106	3.91	3.26	3.26	3.26	4.81	3.75
Proposed controller	0.0059	1.86	1.56	1.56	1.56	2.41	2.18

Table 11: Comparative analysis of the system in terms of peak over/undershoot case 4.

Controller	Peak undershoot (*-ve*)						Peak overshoot					
	Δf_1	Δf_2	Δf_3	Δf_4	$\Delta P_{tie,12}$	ACE_1	Δf_1	Δf_2	Δf_3	Δf_4	$\Delta P_{tie,12}$	ACE_1
FOF-PID optimized via FA	0.0092	0.0060	0.0060	0.0060	0.0021	0.0083	0.0015	0.0013	0.0013	0.0013	0.0002	0.0007
FOF-PID optimized via PSO	0.0077	0.0045	0.0045	0.0045	0.0016	0.0064	0.0016	0.0007	0.0007	0.0007	0.0001	0.0005
FOF-PID optimized via CPSO	0.0086	0.0043	0.0043	0.0043	0.0014	0.0061	0.0021	0.0011	0.0011	0.0011	0.0	0.0006
Proposed controller	0.0069	0.0039	0.0039	0.0039	0.0013	0.0060	0.0020	0.0004	0.0004	0.0004	0.0	0.0001

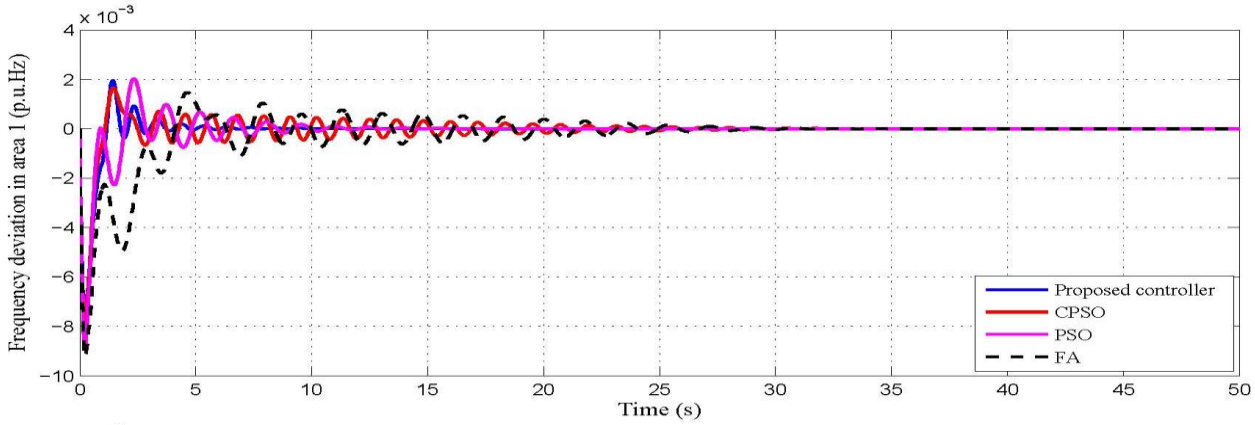

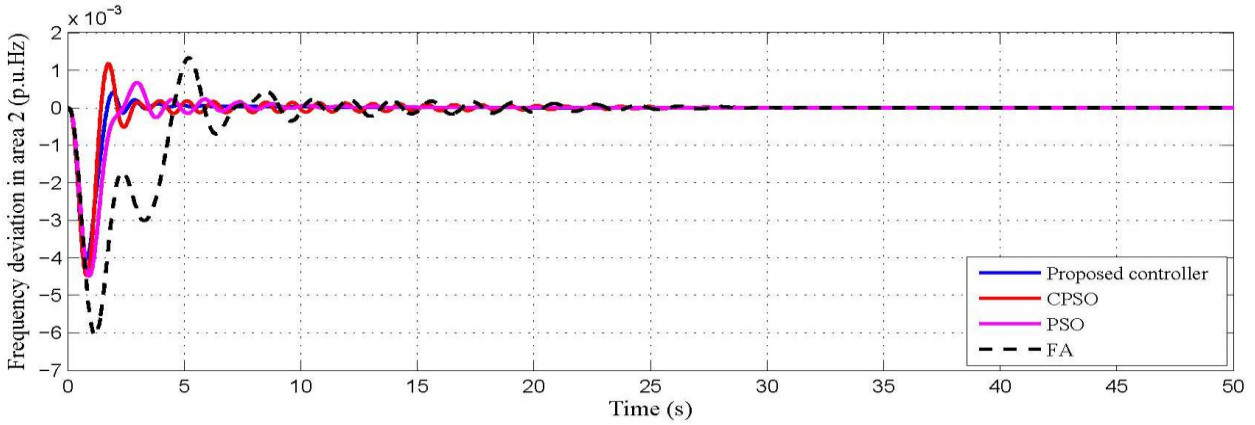

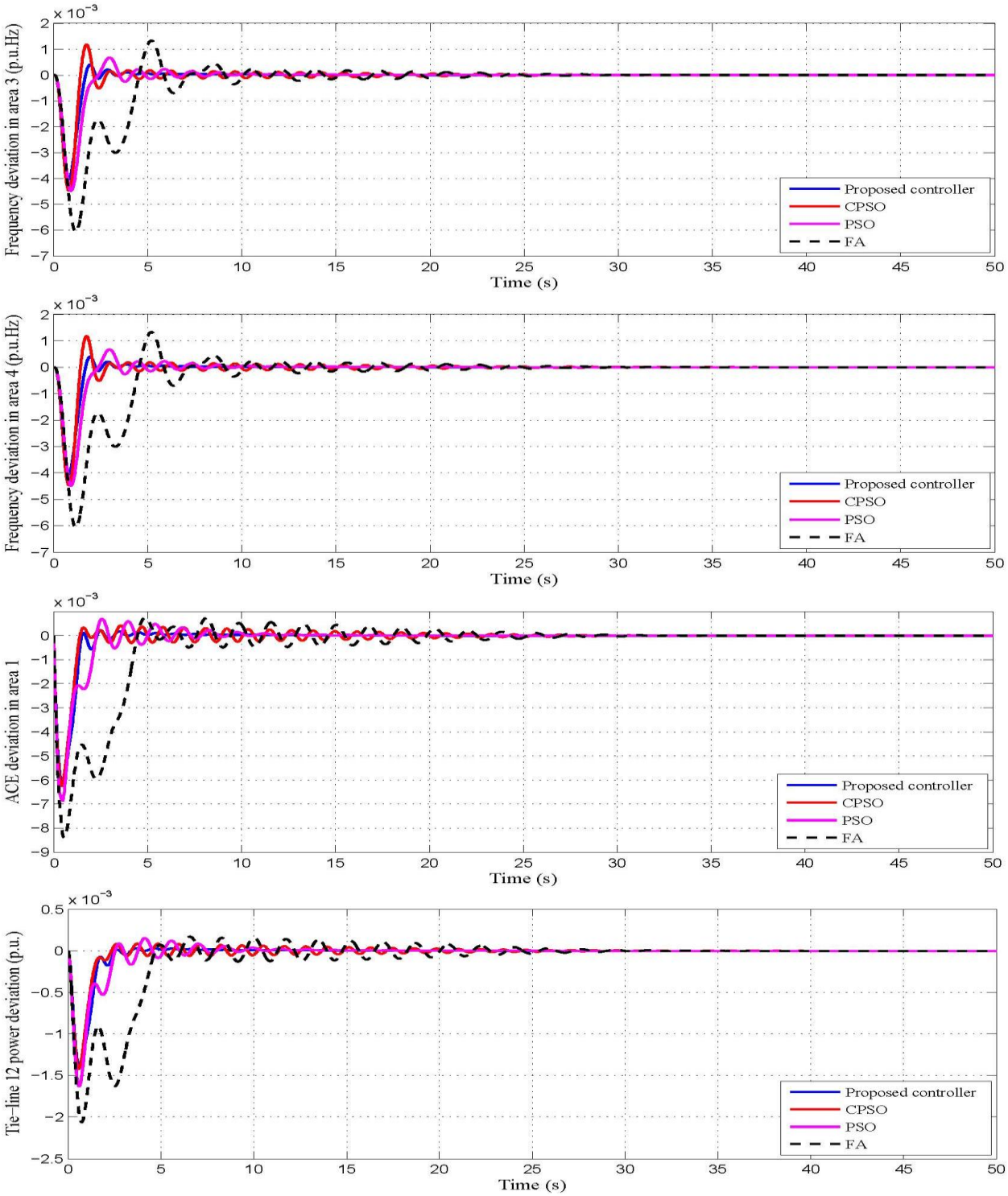

Fig. 12. Comparative dynamic performances of the plant with nonlinearities after 10% SLP in area-1 frequency deviations in area 1, 2, 3, 4 respectively, area control error deviation in area-1, and tie-line power $\Delta P_{tie,12}$ deviation.

VI. Conclusion

In this article, a hybrid firefly and particle swarm optimization (hFA-PSO) is employed for training fractional order fuzzy PID (FOF-PID) controller based LFC of interconnected multi-area power plants. A hFA-PSO is used for regulating the optimal gains of the proposed controller such that minimizing the ITSE of the frequency and tie-line power deviations. Then, the proposed controller is incorporated to an interconnected complex power system comprising nonrenewable and renewable energy sources. The obtained results via hFA-

PSO optimized FOF-PID controller is compared with the other reported techniques such as CPSO, PSO, FA for the same interconnected power system. The proposed hFA-PSO technique takes merit of global exploration competences of FA and local exploitation capability of PSO algorithm. The performance specifications, settling time and over shoot/under shoot of the frequency and tie line power deviations are recorded and compared with others. It is observed that the results of the proposed controller based hFA-PSO is preeminence to others techniques. Also, robustness analysis is performed by varying the loading conditions and plant parameters in the range of +50% to -50% from their nominal values. It is shown that the proposed controller optimized via hFA-PSO approach outperforms to the others approaches. Finally, the obtained results performed that the proposed hFA-PSO optimized FOF-PID controller based LFC of interconnected power systems is meaningfully robust in spite considered wide variation in loading conditions and system parameters.

Acknowledgments: This work was supported by the University of Nyala. The authors wish to thank the anonymous reviewers and the editors for providing valuables comments to improve the quality of the manuscript.

References:

[1]. Gomaa Haroun A. H. and Li Y. Y., A novel optimized hybrid fuzzy logic intelligent PID controller for an interconnected multi-area power system with physical constraints and boiler dynamics, ISA Transactions, , 2017, vol. 71, pp. 364-379.
[2] Gomaa Haroun AH, Yin-Ya L. A novel optimized fractional-order hybrid fuzzy intelligent PID controller for interconnected realistic power systems. Transactions of the Institute of Measurement and Control. 2019; 41(11):3065-80.
[3] Gomaa Haroun A. H., and Li Y.Y. Ant lion optimized fractional order fuzzy pre-compensated intelligent pid controller for frequency stabilization of interconnected multi-area power systems. Applied System Innovation. 2019; 2(2):17.
[4]. P. C. Pradhan, R. K. Sahu, and S. Panda, Firefly algorithm optimized fuzzy PID controller for AGC of multi-area multi-source power systems with UPFC and SMES, Engineering Science and Technology, an International Journal, 2016, vol. 19, pp. 338-354.
[5]. T. Santy and R. Natesan, Load frequency control of a two area system consisting of a grid connected PV system and diesel generator, Int J Emerg Technol Comput Electron, 2015, vol. 13, pp. 456-461.
[6]. S. M. Abd-Elazim and E. S. Ali, Firefly algorithm-based load frequency controller design of a two area system composing of PV grid and thermal generator, Electrical Engineering, 2018, vol. 100, pp. 1253-1262.
[7]. Y. Arya and N. Kumar, BFOA-scaled fractional order fuzzy PID controller applied to AGC of multi-area multi-source electric power generating systems, Swarm and Evolutionary Computation, 2017, vol. 32, pp. 202-218.
[8]. L. Liu, H. Matayoshi, M. Lotfy, M. Datta, and T. Senjyu, Load frequency control using demand response and storage battery by considering renewable energy sources, Energies, 2018, vol. 11, pp. 3412.
[9]. P. Dahiya, V. Sharma, and R. N. Sharma, Optimal generation control of interconnected power system including DFIG-based wind turbine, IETE Journal of Research, 2015, vol. 61, pp. 285-299.
[10]. J. P. Lopes, R. Almeida, and E. Castronuovo, Optimum generation control in wind parks when carrying out system operator requests, 2006.
[11]. S. Abd-Elazim and E. Ali, Load frequency controller design of a two-area system composing of PV grid and thermal generator via firefly algorithm, Neural Computing and Applications, 2018, vol. 30, pp. 607-616.
[12]. M. K. Alam and F. H. Khan, Transfer function mapping for a grid connected PV system using reverse synthesis technique, in Control and Modeling for Power Electronics (COMPEL), 2013 IEEE 14th Workshop on, 2013, pp. 1-5.
[13]. V. Çelik, M. T. Özdemir, and G. Bayrak, The effects on stability region of the fractional-order PI controller for one-area time-delayed load–frequency control systems, Transactions of the Institute of Measurement and Control, 2016.
[14]. X.-S. Yang, Nature-inspired metaheuristic algorithms: Luniver press, 2010.
[15]. P. Kora and K. S. Rama Krishna, Hybrid firefly and Particle Swarm Optimization algorithm for the detection of Bundle Branch Block, International Journal of the Cardiovascular Academy, 2016, vol. 2, pp. 44-48.
[16]. K. S. Rajesh, S. S. Dash, and R. Rajagopal, Hybrid improved firefly-pattern search optimized fuzzy aided PID controller for automatic generation control of power systems with multi-type generations, Swarm and Evolutionary Computation, 2018.
[17]. S. Ali, G. Yang, and C. Huang, Performance optimization of linear active disturbance rejection control approach by modified bat inspired algorithm for single area load frequency control concerning high wind power penetration, ISA Transactions, 2018, vol. 81, pp. 163-176.

Gomaa Haroun A. H, et. al. "A hybrid Firefly and Particle Swarm Optimized FOF-PID Strategy for Interconnected Multi-area Power System with Renewable Energy Sources." *IOSR Journal of Electrical and Electronics Engineering (IOSR-JEEE)*, 17(3), (2022): pp. 23-42.